[CANCER RESEARCH 64, 952–961, February 1, 2004]

TIMP-1 Alters Susceptibility to Carcinogenesis

Jin-Sae Rhee,[1,2] Robert Diaz,[2] Lidiya Korets,[2] J. Graeme Hodgson,[3] and Lisa M. Coussens[2,4,5]

[1]Medical Scientist Training Program, [2]Cancer Research Institute, Departments of [3]Laboratory Medicine, [4]Pathology, and [5]Comprehensive Cancer Center, University of California, San Francisco, California

ABSTRACT

Tissue inhibitors of metalloproteinases (TIMPs) are a family of multifunctional proteins known to possess a broad range of biological activities, including inhibition of metalloproteinase activity, regulation of proliferation and apoptosis of a variety of cell types, and, depending on the context, differential regulation of angiogenic and inflammatory responses. Elevated mRNA expression of TIMP family members correlates with malignancy and clinical outcome in many human cancer types; however, a protective role for TIMPs also has been observed in various mouse models of human cancer. In the current study, we found distinct spatial-temporal expression patterns for the mRNA of TIMP family members in a mouse model of epithelial carcinogenesis [*i.e.*, keratin 14-human papillomavirus 16 (K14-HPV16) transgenic mice]. To test the hypothesis that elevated expression of TIMP-1 functionally regulates epithelial carcinogenesis, we introduced a human TIMP-1 transgene into K14-HPV16 transgenic mice and assessed neoplastic progression. Results from these studies suggest that TIMP-1 enhances tumorgenicity by potentiating keratinocyte hyperproliferation and appearance of chromosomal aberrations in premalignant cells, thereby increasing their risk to undergo malignant conversion. In addition, TIMP-1 inhibits tissue gelatinolytic activity in tumor stroma, affects stabilization of collagen fibrils, but does not inhibit malignant conversion of dysplasias into carcinomas or development of metastases. The combined implications of these studies suggest that TIMP-1 is an important contributor to epithelial neoplastic progression and supports the concept that TIMP-1 exerts differential regulation on tissues in a stage-dependent manner.

INTRODUCTION

Tissue inhibitors of metalloproteinases (TIMPs) are a family of four multifunctional proteins numbered in order of their discovery and characterized by a conserved structure ranging from M_r 20,000 to 30,000 that inhibits metalloproteinase (MP) activity, specifically matrix metalloproteinase (MMP) activities in a one-to-one stoichiometry (1). Although named for their ability to inhibit MP activity, TIMPs also possess other important bioactivities (2–4). TIMP-1, identified originally for its erythroid-potentiating activity (5), induces proliferation in a wide range of cell types (6–8) by mechanisms that are apparently independent of MMPs (9). In addition, TIMP-1 is known to promote activation of angiogenesis (4, 10, 11), regulate apoptosis (12), amplify inflammation (13), and regulate metastasis formation (14). Similar pleiotropic activities have also been demonstrated for TIMP-2 (15), TIMP-3 (16), and TIMP-4 (17).

TIMP-1 mRNA expression is up-regulated in many human cancer types and in some cases correlates with more severe clinical outcome (*e.g.*, colorectal carcinoma, non-small cell lung carcinoma and breast carcinoma; Ref. 18). Studies in experimental mouse models have revealed paradoxically that TIMP-1 can exhibit proneoplastic and antineoplastic effects during primary and metastatic tumor development (14, 19–24).

In the current study, we have sought to critically examine the spatial-temporal expression patterns of TIMP mRNA and to evaluate the functional significance of TIMP-1 expression during *de novo* epithelial carcinogenesis using a transgenic mouse model of skin carcinoma development [*e.g.*, keratin 14-human papillomavirus 16 (K14-HPV16) transgenic mice; Refs. 25–27]. In K14-HPV16 transgenic mice, the expression of HPV16 early region genes has been targeted to basal keratinocytes (28); animals are born phenotypically normal, and by age 1 month with 100% penetrance, transgenic skin becomes uniformly hyperplastic. These benign lesions advance focally into broad hyperproliferative dysplastic lesions present in 100% of mice age 4–6 months. By age 1 year, ~60% of mice develop tumors, 50% of which are squamous cell carcinomas (SCCs) that metastasize to regional lymph nodes with an ~30% frequency and 10% of which are locally invasive nonmetastatic microcystic adnexal carcinomas (MACs). Results from the current study suggest that TIMP mRNAs are not regulated coordinately during the development and progression of skin carcinogenesis in HPV16 mice and that sustained TIMP-1 expression functionally promotes epithelial carcinogenesis during the early stages of neoplastic progression, whereas in later stages, it inhibits tissue gelatinolytic activity and stabilizes extracellular matrices (ECMs) without affecting metastatic spread.

MATERIALS AND METHODS

Animal Husbandry, Genotype, and Histopathologic Analyses. K14-HPV16 transgenic mice (28), the preparation of tissue sections for histologic examination, and the characterization of neoplastic stages based on H&E histopathology and keratin intermediate filament expression have been described previously (25–27, 29). Tissue samples were fixed by immersion in 10% neutral buffered formalin, dehydrated through graded ethanol and xylenes, embedded in paraffin, cut by a Leica 2135 microtome (Wetzlar, Germany) into 5-μm-thick sections, and histopathologically examined after H&E staining and immunoreactivity of keratin intermediate filaments. Hyperplastic lesions were identified by a twofold increase in epidermal thickness and an intact granular cell layer with keratohyalin granules; dysplastic lesions were characterized based on basal and spinous cell layers with hyperchromatic nuclei representing more than half of the total epidermal thickness and incomplete terminal differentiation of keratinocytes; and SCC lesions were noted by an abundance of abnormal mitotic figures and an invasive loss of integrity in the basement membrane with clear development of malignant cell clusters proliferating in the dermal stroma. Characterization of infundibular (MACs) and sebaceous lesions (sebaceous adenomas) was as described previously (27).

The βA-hT1 transgenic mice have been described previously (30). Briefly, these mice contain a transgene in which the human β-actin promoter directs expression of a human TIMP (hTIMP)-1 cDNA, generated initially in the CD1 mouse strain. To minimize the effect of background strain differences in susceptibility to carcinogenesis, βA-hT1 mice were backcrossed a minimum of six generations into the FVB/n strain before intercrossing with K14-HPV16 mice (FVB/n, N15). The βA-hT1 transgene was followed by PCR genotyping of tail DNA using oligonucleotide primers (5′-TGTGGGACACCAGAAGTCAAC-3′ and 5′-CTATCTGGGACCGCAGGGACT-3′). DNA was amplified for 30 cycles at 95°C for 60 s, 59°C for 30 s, and 72°C for 120 s to generate a 480-bp product corresponding to a region within the hTIMP-1 cDNA. In all of the analyses, HPV16/βA-hT1$^+$ double transgenic mice were compared with littermate control mice lacking the βA-hT1 transgene (HPV16/βA-hT1$^-$). P values ≤ 0.05 were considered to be statistically significant.

Received 8/6/03; revised 10/20/03; accepted 11/4/03.

Grant support: J-S. Rhee was supported by the UCSF Medical Scientist Training Program and a UC Regents Fellowship. L. M. Coussens was supported by grants from the National Cancer Institute, The Hellman Family, and the American Association for Cancer Research.

The costs of publication of this article were defrayed in part by the payment of page charges. This article must therefore be hereby marked *advertisement* in accordance with 18 U.S.C. Section 1734 solely to indicate this fact.

Requests for reprints: Lisa M. Coussens, Comprehensive Cancer Center, University of California, San Francisco, 2340 Sutter Street, San Francisco, CA 94143. E-mail: coussens@cc.ucsf.edu.

RNA Analysis. Real-time PCR analysis was performed as described previously (27). Total RNA was extracted with TRIzol reagent (Invitrogen, Carlsbad, CA) according to the manufacturer's recommendations and the method of Chomczynski (31) by powdering fresh-frozen tissue samples in liquid nitrogen, homogenizing with a microtube pestle (USA Scientific, Ocala, FL), and shearing by multiple passages through a syringe and 21-gauge needle (Becton Dickinson, Franklin Lakes, NJ), followed by phenol-chloroform extraction and isopropanol precipitation. Quantification of TIMP-1 mRNA levels was performed on three mice per category as described previously (27).

In situ hybridization was performed as described previously (25) using ^{35}S-labeled riboprobes generated from cDNA containing plasmid templates for mouse TIMP-1 (32), mouse TIMP-2 (33), mouse TIMP-3 (34), mouse TIMP-4 (35), and hTIMP-1 (30). As negative controls, hybridization using sense probes was performed and showed no signal (data not shown).

Protein Analysis. Protein lysates were prepared by grinding fresh-frozen tissue samples from ear, tumor, or lymph nodes in liquid nitrogen and homogenizing in Tris buffer [25 mM Tris (pH 7.6), 5 mM $CaCl_2$, and 0.25% Triton X-100] in a 2-ml tissue grinder (Fisher Scientific, Hampton, NH). After centrifugation at 13,000 × *g* at 4°C for 30 min, supernatants were measured for protein concentration by the detergent-compatible protein assay (Bio-Rad, Hercules, CA). Serum samples were prepared by extraction of whole blood, coagulated overnight at 4°C, followed by centrifugation at 700 × *g* at 4°C for 30 min to remove cells. ELISA was performed in 96-well Costar plates (Corning, Corning, NY) prepared by precoating with a mouse monoclonal anti-hTIMP-1 antibody (Oncogene Research Products, Boston, MA) diluted 1:250 in 50 mM carbonate buffer (pH 9.6) at 4°C overnight, followed by blocking in 1% BSA in PBS at room temperature for 1 h. Plates were washed with buffer (0.1% BSA, 0.05% Tween-20, in PBS) and incubated with either 10 μl serum or 25 μg protein lysate diluted in wash buffer for 3 h. Plates were washed and then processed by incubation with a rabbit polyclonal anti-hTIMP-1 antibody (Biogenesis, Kingston, NH) diluted 1:1,000 in wash buffer, goat antirabbit biotinylated secondary antibody (Pierce Biotechnology, Rockford, IL) diluted 1:10,000 in wash buffer, and ExtrAvidin peroxidase conjugate (Sigma Chemical Co., St. Louis, MO) diluted 1:1,000 in blocking buffer. Assays were performed with the Quantikine detection system (R&D Systems, Minneapolis, MN) by the manufacturer's recommendations and quantified at 650 nm on a SpectraMax 340 spectrophotomoter (Molecular Devices Corp., Sunnyvale, CA). Samples were assayed from three mice per category, and all of the experiments were repeated three times.

Gelatinase Assay. Protein lysates were generated from fresh-frozen tissue samples as described previously for the ELISA assay. Three μg of protein lysate were incubated at 37°C in reaction buffer [50 mM Tris (pH 7.6), 150 mM NaCl, 5 mM $CaCl_2$, 0.2 mM NaN_3, and 0.05% Brij-35] with 400 ng DQ-gelatin (Molecular Probes, Eugene, OR) in a total volume of 200 μl/well in a 96-well black tissue culture microtiter plate (Becton Dickinson). Reactions were incubated for up to 5 h at 37°C, and fluorescence was measured (excitation, 485 nm; emission, 530 nm) every 3 min on a SpectraMax Gemini spectrophotometer (Molecular Devices Corp.) operated by SoftMax Pro 4.3 software (Molecular Devices Corp.). MMP inhibition was performed by incubation in the presence of 4 mM 1,10-phenanthroline (Sigma Chemical Co.). Tissue lysates from four mice were assayed per category, and all of the experiments were repeated three times.

Substrate Zymography. Tissue samples from negative littermate or neoplastically staged transgenic mice were weighed and then homogenized (1:8 ratio of weight to volume) in lysis buffer containing 50 mM Tris-HCl (pH 8.0), 150 mM NaCl, 0.1% NP-40, 0.5% deoxycholate, and 0.1% SDS. Soluble and insoluble extracts were separated by centrifugation (10,000 × *g*) and subsequently stored at −80°C. Equivalent amounts of soluble extract were analyzed by gelatin zymography on 10% SDS-polyacrylamide gels copolymerized with substrate (1 mg/ml of gelatin) in sample buffer [2% SDS, 50 mM Tris-HCl, 10% glycerol, and 0.1% bromphenol blue (pH 6.8); Ref. 36]. After electrophoresis, gels were washed three times for 30 min in 2.5% Triton X-100 and three times for 15 min in ddH_2O, incubated overnight at 37°C in 50 mM Tris-HCl and 10 mM $CaCl_2$ (pH 8.2), and then stained in 0.5% Coomassie Blue and destained in 20% methanol and 10% acetic acid. Negative staining indicates the location of active protease bands. Exposure of proenzymes within tissue extracts to SDS during the gel separation procedure leads to activation without proteolytic cleavage (37).

Picrosirius Red Staining. Staining of collagen in tissues by picrosirius red was performed as described previously (38, 39). Five-μm-thick paraffin sections were deparaffinized in xylenes, rehydrated in graded ethanol, and stained for 1 h in 0.1% (w/v) solution of sirius red F3B dissolved in saturated aqueous picric acid. Sections were rinsed in 0.5% glacial acetic acid, dehydrated in graded ethanol and xylenes, and mounted in Cytoseal 60 (Fisher Scientific). Images were captured at high magnification under normal illumination and polarized light on a Leica DM-RXA microscope attached to a Leica digital camera operated by OpenLab software (Improvision). Presence of mature fibrillar type I collagen was assessed from captured images (40, 41) using the morphometric quantification technique described previously (42). For each field, an image taken under polarized light was quantified for pixel density using a set threshold for detection of the strongly birefringent signal indicative of fibrillar collagen. For the same field, an image under brightfield was quantified for exclusion of regions not to be evaluated (*i.e.*, vessel lumen, ear cartilage, and epithelial compartments). Calculated values represent the percentage of fibrillar collagen, normalized for stromal area, and averaged from four fields per mouse with six mice per category.

Immunohistochemistry. Immunohistochemical detection of antigens was performed as described previously (25). To simultaneously detect keratin 5 and bromodeoxyuridine (BrdU)-positive cells in tissues, animals received i.p. injections of BrdU (Roche, Basel, Switzerland) dissolved in PBS at 50 μg/g total body weight 90 min before animals were killed and tissue samples were prepared. Five-μm-thick paraffin sections were deparaffinized in xylenes, rehydrated in graded ethanol, boiled in Citra antigen-retrieval solution (BioGenex, San Ramon, CA), washed in PBS, blocked in 1× blocking buffer (5% normal goat serum/2.5% BSA and PBS), and incubated in a 1:10,000 dilution of a rabbit polyclonal antibody against mouse keratin 5 (Babco, Richmond, CA) in 0.5× blocking buffer overnight at 4°C, followed by a series of PBS washes, incubation of slides with a biotinylated donkey secondary antibody against rabbit (Pierce), blocking in 0.6% hydrogen peroxide in methanol, conjugation by ABC-Elite (Vector, Burlingame, CA), and development in Fast-DAB (Sigma Chemical Co.). BrdU-positive cells were detected essentially as described by the manufacturers' recommendations using the BrdU Labeling Kit II (Roche), developed by Vector Red Alkaline Phosphatase Kit (Vector), counterstained by H&E, dehydrated by graded ethanol and xylenes, and mounted in Cytoseal 60 (Richard-Allan Scientific, Kalamazoo, MI). Five fields per mouse were captured at high magnification (40×) on a Leica DM-RXA microscope attached to a Leica digital camera operated by OpenLab software (Improvision, Lexington, MA). Proliferative index was quantified from five high-power (40×) images per tissue and included five mice per category as the percentage of the BrdU-positive nuclei in keratin 5-positive keratinocytes over the total number of keratin 5-positive keratinocytes.

Apoptotic frequency was assayed on 5-μm-thick paraffin sections, deparaffinized as described previously, and processed for the terminal deoxynucleotidyl transferase-mediated nick end labeling reaction using the fluorescein-FragEL DNA fragmentation detection kit (Oncogene Research Products) by the manufacturer's recommendations. Apoptotic index was quantified from five high-power (40×) images per tissue and included five mice per category as the percentage of the terminal deoxynucleotidyl transferase-mediated nick end labeling-positive keratinocytes over the total number of 4′,6-diamidino-2-phenylindole-stained keratinocytes.

Dual-Color Fluorescent in Situ Hybridization (FISH) on Paraffin Sections

Preparation of Paraffin Sections. Neoplastically staged tissue sections were deparaffinized by incubating slides at 65°C for 30 min on a heating block, followed by three incubations in xylene for 15 min at 50°C. Xylene was removed by three washes in 100% ethanol for 5 min at room temperature. After rehydration (2-min washes in 85%, 70%, and 50% ethanol), slides were rinsed in 1× PBS at room temperature, incubated in 1M NaSCN for 8 min at 80°C, and washed two times in 1× PBS for 5 min at room temperature. The sections were digested with 0.1 mg/ml pepsin (Worthington Biochemicals, Lakewood, NJ) for 4 min at 37°C, rinsed with 1× PBS at 4°C, washed in 1× PBS/0.1% Tween-20 for 5 min at room temperature, and rinsed in ice cold 1× PBS. The sections then were dehydrated (2 min each in 70%, 85%, and 100% ethanol), air dried for 15 min at 37°C, fixed in Carnoy's solution (3:1 ratio of methanol and acetic acid), and air dried for 30 min at 37°C. In preparation for hybrid-

ization, sections were rehydrated, incubated in 2× SSC for 30 min at 37°C, denatured in 50% formamide/2× SSC for 5 min at 37°C, dehydrated, and then placed on a 37°C slide warmer until the hybridization mixture was added. Once fluorescent *in situ* hybridization (FISH) probes were placed on sections, the sections were covered with plastic cover strips and placed in plastic slide holders (American Scientific, Columbus, OH) containing a strip of Whatman paper (3 mm) soaked in 750 μl of 50% formamide/2× SSC (pH 7.0). After hybridizing for 48–72 h at 37°C, the slides were washed in three 10-min washes consisting of 50% formamide/2× SSC at 45°C, one 10-min wash in 2× SSC at 45°C, one 10-min wash in 2× SSC at room temperature, one 10-min wash in 4× SSC/0.1% Trition X-100 at room temperature, and two 5-min washes in ddH_20 at room temperature. The sections then were counterstained with 1.0 μM 4′,6-diamidino-2-phenylindole (Sigma Chemical Co.) in 90% glycerol/1× PBS mounting solution.

Preparation of Hybridization Probes. Probes mapping to consistently amplified regions of chromosome 5 (clone RP23–451L8, coordinates 74787760 bp to 74991110 bp and clone RP23–118A6, coordinates 17908843 bp to 18113246 bp; BAC PAC Resource Center at the Children's Hospital Oakland Research Institute, Oakland, CA), and unchanged regions (chromosome 10 clone CITB-CJ7B-047K7 containing marker D10MIT49 at coordinates 6066401 bp to 6066505 bp, and clone RP23–421E11, coordinates 81701304 bp to 81701622 bp; BAC PAC Resource Center at the Children's Hospital Oakland Research Institute) as determined by array comparative genomic hybridization analyses were selected. All of the coordinates are based on the February 2003 freeze of the mouse genome assembly at http://genome.ucsc.edu. DNA templates for FISH probes (200 ng) were digested with *Dpn*II (New England Biolabs, Beverly, MA), purified with QiaQuick PCR purification columns (Qiagen, Valencia, CA), and random prime-labeled using the BioPrime DNA Labeling kit (Invitrogen) with either Cy3-dUTP (Amersham Biosciences, Piscataway, NJ) or Alexa 488-dUTP (Molecular Probes). The labeled samples were purified separately using G-50 mini-spin columns (Amersham), coprecipitated with 50 μg of mouse Cot-1 DNA (Invitrogen), and resuspended in 20 μl of hybridization buffer (50% formamide/2× SSC/10% dextran sulfate/2% SDS) before denaturation at 72°C for 15 min.

Analysis. Quantification was performed using a Zeiss Axioplan microscope (Oberkochen, Germany) at 100× magnification under oil immersion. From the ventral ear leaflet of each animal, 50 labeled nuclei were counted from a minimum of four mice per time point. The data shown reflect the percentage of an average copy number ratio of chromosome 5 (Cy3 signals) to chromosome 10 (Alexa 488 signals) for each animal. To optimize the sensitivity for the low copy number changes in hyperplasias, scoring was limited to nuclei of basal keratinocytes that were within the first two cell layers adjacent to the basement membrane that demonstrated hybridization signals for both fluorochromes.

RESULTS

TIMP-1 mRNA Expression Increases during Neoplastic Progression in HPV16 Transgenic Mice. In studies of human cancer, many groups have documented increased expression of hTIMP-1 mRNA as compared with adjacent premalignant or distal normal control tissue (32, 43, 44). Using K14-HPV16 transgenic mice, we sought to examine the spatial and temporal expression patterns of TIMP family members during epithelial neoplastic progression and to determine the functional significance of TIMP-1 during that progression (25, 28). We used real-time PCR to quantify the amount of TIMP-1 mRNA in tissue samples representing distinct stages of neoplastic development (*i.e.*, hyperplastic, dysplastic, and SCCs) as compared with normal skin (Fig. 1*A*). These data revealed an incremental increase in TIMP-1 mRNA at each neoplastic stage similar to reports for human carcinoma development (32, 43, 44).

To determine the spatial and temporal expression patterns of TIMP-1 mRNA expression in neoplastic skin, we used *in situ* hybridization analysis on neoplastically staged paraffin-embedded tissue sections (Fig. 1, *B–G*). Whereas TIMP-1 mRNA was not observed in non-neoplastic normal skin (Fig. 1*B*), it was detected diffusely within the epidermis and focally in discrete areas of the dermal stroma in hyperplasias and dysplasias (Fig. 1, *C* and *D*). In contrast to the diffuse expression in premalignant tissue, expression of TIMP-1 mRNA was increased focally in malignant keratinocytes at the invasive edges of Grade I and Grade III SCCs with persistent low-level expression in tumor-associated stromal cells (Fig. 1, *E* and *F*). TIMP-1 mRNA was not observed in lymph nodes with or without SCC metastases (Fig. 1*G*).

TIMP mRNAs Are Not Coordinately Regulated during Squamous Carcinogenesis. mRNA expression of TIMP family members is known to be regulated differentially during embryonic development (3) and in some pathologic disease states (45). To determine whether

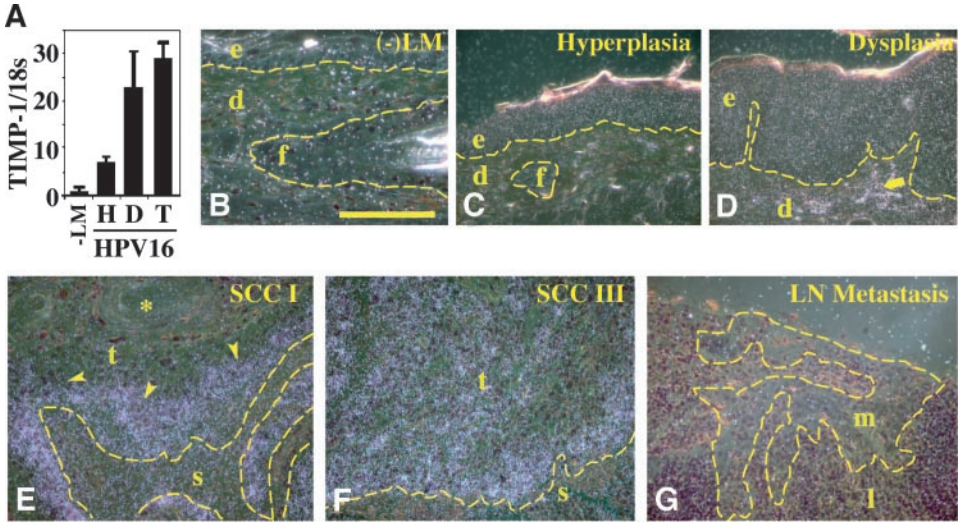

Fig. 1. Tissue inhibitors of metalloproteinase (*TIMP*)-1 mRNA expression during squamous carcinogenesis in human papillomavirus-16 (*HPV16*) transgenic mice. *A*, real-time PCR analysis of TIMP-1 mRNA. Total RNA was obtained from ears of negative littermates (*−LM*), premalignant hyperplastic (*H*) and dysplastic (*D*) epidermis, and squamous cell carcinomas (SCCs) from keratin 14 (*K14*)-HPV16 mice (*T*). Real-time PCR for endogenous mouse TIMP-1 mRNA was performed and calculated as a ratio over 18S rRNA as a standard. Error bars represent SEM *B–G*, Spatial-temporal expression of TIMP-1 mRNA during neoplastic progression. An antisense riboprobe specific for mouse TIMP-1 mRNA was hybridized to paraffin-embedded neoplastically staged tissue sections from negative littermate ears (*B*); ears from HPV16 mice with hyperplastic (*C*), dysplastic (*D*), and SCC pathologies; Grade I SCC (*E*); Grade III SCC (*F*); and axillary lymph nodes containing metastases (*G*). *Arrowheads* indicate silver grains corresponding to epithelial cells expressing TIMP-1 mRNA; *arrows* indicate silver grains corresponding to stromal cells expressing TIMP-1 mRNA; *dashed lines* denote the epidermal-dermal or keratinocyte-stromal boundaries. e, epidermis; d, dermis; f, hair follicle; t, tumor; s, stroma; ∗keratin pearl; m, metastasis; and l, lymphoid tissue. Scale bar: 100 μm (*B*), 160 μm (*C, D,* and *G*), and 256 μm (*E* and *F*).

the mRNAs for TIMP-2, -3, or -4 were expressed coordinately with TIMP-1 (spatially and/or temporally), mRNA expression of TIMP-2, -3, and -4 was examined on adjacent tissue sections by *in situ* hybridization analysis (data not shown), which demonstrated TIMP-2 and -3 mRNA expression in follicular epithelial and ear pericartilage cells in negative littermate skin, whereas in neoplastic skin, their expressions were increased incrementally in neoplastic keratinocytes throughout neoplastic progression and were most prominent in Grade I well-differentiated SCCs. Expression of TIMP-4 mRNA was not observed in either wild-type skin or any of the neoplastic stages from HPV16 mice. These data suggest that TIMP-2, -3, and -4 mRNAs are not expressed coordinately with TIMP-1 mRNA during squamous epithelial carcinogenesis.

TIMP-1 Enhances Epithelial Carcinogenesis. The progressive increase and distinctive spatial expression pattern of TIMP-1 mRNA observed during neoplastic progression in HPV16 mice suggested that TIMP-1 might contribute functionally to neoplastic development by mechanisms distinct from those regulated by TIMP-2 or -3. To test this hypothesis and to assess the functional significance of increased TIMP-1 mRNA expression during neoplastic progression, we took a genetic approach using TIMP-1 transgenic mice wherein a hTIMP-1 cDNA was regulated by the human β-actin promoter (*i.e.,* βA-hT1$^+$ transgenic mice; Ref. 30). K14-HPV16 transgenic mice were intercrossed with βA-hT1$^+$ mice to generate two cohorts: single transgenic control (HPV16/βA-hT1$^-$; $n = 83$) and double transgenic mice (HPV16/βA-hT1$^+$; $n = 129$).

Histopathologically, HPV16/βA-hT1$^-$ control mice were indistinguishable phenotypically from historical HPV16 transgenic cohorts ($n = 297$; Ref. 27). With 100% penetrance, HPV16/βA-hT1$^-$ mice developed hyperplastic skin that was visually discernible at weaning, followed by development of focal dysplasias between 4 and 6 months of age (Fig. 2*B*). HPV16/βA-hT1$^-$ mice exhibited a similar latency and incidence of SCC (~55%) and MAC (~10%) development by 12 months of age as historical HPV16 control cohorts (27), with the earliest cancers also occurring by ~4 months of age (Fig. 2, *A* and *B*).

Although not altering the latency of progression between neoplastic stages, expression of hTIMP-1 in HPV16/βA-hT1$^+$ mice (Fig. 2, *A* and *B*) resulted in a significantly increased incidence of tumors (*e.g.,* papillomas, sebaceous adenomas, SCCs, and MACs; 83.0% *versus* 65.1% in HPV16/βA-hT1$^-$ mice; $P = 0.0048$, log-rank analysis; Fig. 2, *A* and *B*), whereas anatomic location and tumor multiplicity were unchanged (data not shown). Histopathologic analysis of HPV16/βA-hT1$^+$ skin tumors revealed that their increased number was caused by an increased incidence of SCCs (64.3% *versus* 55.4% in HPV16/βA-hT1$^-$ mice; $P = 0.0342$, log-rank analysis) and MACs (21.7% *versus* 10.8% in HPV16/βA-hT1$^-$ mice; $P = 0.0131$, log-rank analysis), whereas SCC grade (Fig. 2*C*) and frequency of lymphatic metastases were not significantly different between the two cohorts (Fig. 2*B*).

Decreased MMP Activity and Increased Matrix Stability in HPV16/βA-hT1$^+$ Mice. The observed increase of SCCs and MACs in HPV16/βA-hT1$^+$ mice suggested that TIMP-1 potentiated the frequency of malignant conversion; however, the underlying biological mechanisms involved in this potentiation were not clear.

To determine how presence of hTIMP-1 protein correlated with altered neoplastic progression in HPV16/βA-hT1$^+$ mice, we first used an ELISA to determine the amount of hTIMP-1 in (non-HPV16) βA-hT1$^+$ *versus* βA-hT1$^-$ serum (Fig. 3*A*) and in neoplastically staged tissue lysates from HPV16/βA-hT1$^+$ mice and found that hTIMP-1 protein increased from ~0.5 ng/mg in hyperplastic skin to ~1.5 ng/mg in carcinomas (Fig. 3*B*). Because the most notable bioactivity (at high concentrations) of TIMP-1 is its ability to inhibit MP activity (1), we asked whether the increased levels of hTIMP-1 in dysplasias and/or SCCs altered MP activity in those tissues. To test this, we used an *in vitro* gelatinase assay to determine total gelatinolytic activity in HPV16/βA-hT1$^+$ and HPV16/βA-hT1$^-$ tissues derived from distinct stages of neoplastic progression (Fig. 3*C*). In early hyperplastic and dysplastic tissues, gelatinolytic activity was not significantly different between lysates derived from the two cohorts

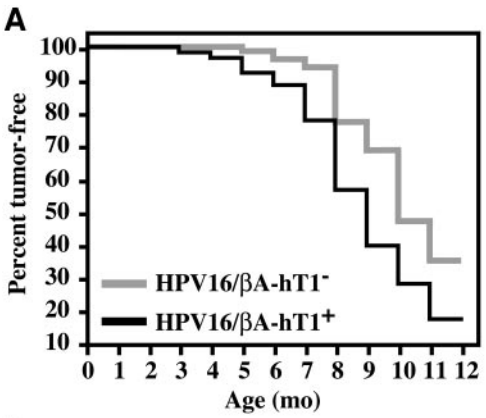

B

Histopathology	HPV16/βA-hT1- n = 83	HPV16/βA-hT1+ n = 129	p value (log rank)
Hyp (by 1-mo)	100	100	
Dys (by 6-mo)	100	100	
Skin Tumor	65.1	83.0	0.0048
Papilloma	13.2	12.4	
SA	6.0	5.4	
SCC	55.4	64.3	0.0342
MAC	10.8	21.7	0.0131
LN mets	23.2	17.2	

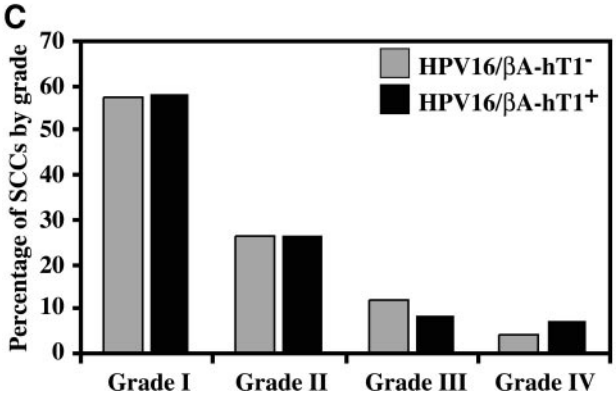

Fig. 2. Increased tumorgenicity in human papillomavirus-16 (*HPV16*)/βA-hT1$^+$ mice. *A,* tissue inhibitors of metalloproteinase (TIMP)-1 increases tumorgenicity in HPV16 mice. Cohorts of HPV16/βA-hT1$^-$ ($n = 83$) and HPV16/βA-hT1$^+$ mice ($n = 129$) were aged 12 months or until appearance of tumors as found by gross examination, whereupon tissues were assessed histopathologically by H&E staining and keratin intermediate filament immunoreactivity to detect the presence and nature of malignant lesions. Curves reflect the percentage of tumor-free mice in each cohort, wherein mice developing papillomas, sebaceous adenomas, squamous cell carcinomas (*SCCs*) or microcystic adnexal carcinomas (*MACs*) were counted as tumor bearing. A statistically significant difference was found when comparing the two cohorts ($P = 0.0048$, log-rank analysis). *B,* incidence of specific epithelial neoplasms. Tissue sections from the two cohorts were analyzed by H&E staining and keratin intermediate filament immunoreactivity to determine the incidence of mice developing hyperplastic skin by 1 month of age (*Hyp*); dysplasia by 6 months of age (*Dys*); lifetime incidence of skin tumors including papillomas, sebaceous adenomas (*SA*), SCCs, and MACs; and incidence of mice with metastatic tumors in sentinel lymph nodes (*LN mets*). Values represent percentages of mice with that particular neoplastic phenotype, and statistically significant differences between the two cohorts are shown. *C,* distribution of SCCs by grade. Tissue sections of SCCs from the two cohorts were analyzed by H&E histopathology and keratin intermediate filament immunoreactivity to determine the grade of each carcinoma based on its relative differentiation characteristics. Values represent the percentage for each SCC grade as a fraction of the total number of SCCs within each cohort.

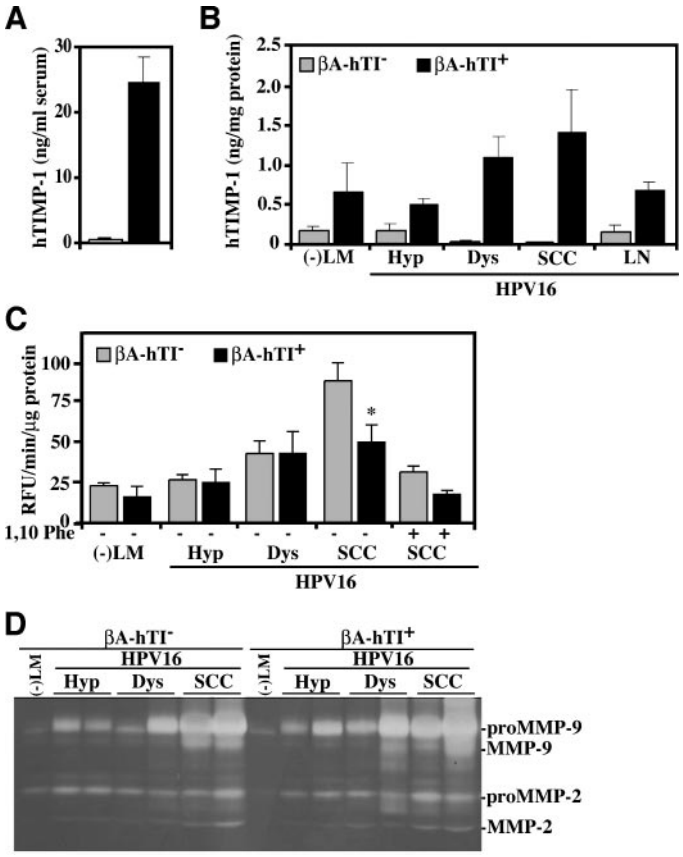

Fig. 3. Increased tissue inhibitor of metalloproteinase (*TIMP-1*) expression decreases tissue gelatinolytic activity. *A*, serum levels of human TIMP-1 (*hTIMP-1*) protein in transgenic mice. ELISA was performed on serum from βA-hT1$^-$ (*gray bar*) and βA-hT1$^+$ (*black bar*) mice using antibodies specific for hTIMP-1. Values represent hTIMP-1 protein (hTIMP-1) in serum (ng/ml) compared with recombinant hTIMP-1 as a control and averaged for three mice per category. Error bars represent SE. *B*, tissue levels of transgenic hTIMP-1 protein in human papillomavirus-16 (*HPV16*) transgenic mice. ELISA was performed on tissue extracts from ears of negative littermate (−*LM*) mice, premalignant ears with hyperplasia (*Hyp*) or dysplasia (*Dys*), squamous cell carcinoma (*SCC*), and lymph nodes (*LN*) from HPV16/βA-hT1$^-$ and HPV16/βA-hT1$^+$ mice, as described in (*A*). Values represent hTIMP-1 protein in tissue (ng/mg) averaged for three mice per time point. Error bars represent SE. *C*, gelatinase activity in neoplastic tissues. Enzymatic solution assays were performed on tissue extracts representing the same categories as in (*B*). Gelatinolytic activities in tissue extracts were measured by incubation with fluorescein-conjugated gelatin, in the absence or presence of the metalloproteinase inhibitor 1,10 phenanthroline (4 mM). Values represent the change in relative fluorescence units (*RFU*)/min/μg tissue protein averaged for four mice per time point. Error bars represent SE, and ∗denote statistically significant differences between the HPV16/βA-hT1$^-$ and HPV16/βA-hT1$^+$ categories ($P = 0.0392$, Mann-Whitney test). *D*, gelatin substrate zymography of neoplastic tissue lysates. Tissue lysates were prepared from −LM and HPV16/βA-hT1$^-$ and HPV16/βA-hT1$^+$ mice with distinct neoplastic development and assessed for relative differences in levels of pro and/or active molecular weight forms of matrix metalloproteinase (*MMP*)-2 and MMP-9, which were not found to vary between the two genotypes.

(Fig. 3*C*). In contrast, carcinoma tissue lysates derived from HPV16/βA-hT1$^-$ skin had an increase in total gelatinolytic activity compared with lysates from histopathologically similar HPV16/βA-hT1$^+$ carcinomas (89.5 *versus* 51.1 relative fluorescence units/min/μg; $P = 0.0392$, Mann-Whitney two-tailed analysis; Fig. 3*C*) but did not demonstrate any changes in abundance of either pro or active species of MMP-2 and MMP-9 (Fig. 3*D*). In combination, these data suggested that increased hTIMP-1 levels in HPV16/βA-hT1$^+$ carcinomas (~1.5 ng/mg) were sufficient to inhibit gelatinolytic activity present in SCCs by post-translational inhibition of gelatinolytic MMPs and/or other MP family members.

To assess functionally whether ECM architecture was altered in HPV16/βA-hT1$^+$ dysplasias and/or carcinomas resulting from decreased gelatinolytic activity *in vivo*, we examined histologically the status of collagen fibrils *in situ* by picrosirius red staining (39, 40), an analysis that allows distinction between thinner reticular collagen *versus* thicker collagen fibrils based on colored birefringence differences (Fig. 4; Refs. 40 and 41). Qualitatively, polarization microscopic analysis of the picrosirius red staining in dysplasias and carcinomas from HPV16/βA-hT1$^-$ mice suggested that stroma adjacent to dysplasias (Fig. 4*A*) and tumor nests (Fig. 4*C*) contained a combination of thick and thin collagen fibers that were predominately weakly birefringent. In contrast, in HPV16/βA-hT1$^+$ mice, stroma adjacent to dysplastic epidermis (Fig. 4*B*) and within carcinomas (Fig. 4*D*) was almost devoid of thin weakly birefringent collagen fibers but was instead composed predominately of more intensely birefringent thicker fibers. Quantitative morphometric analysis of the picrosirius red staining between the two cohorts was different significantly at the dysplastic and carcinoma stages, with a more than twofold increase in the percentage of the intensely birefringent collagen fibers in the HPV16/βA-hT1$^+$ carcinomas (6.5% *versus* 15.0%; $P = 0.0317$, Mann-Whitney two-tailed analysis) and an ~1.8-fold increase at the dysplastic stage (37.0% *versus* 69.1%; $P = 0.0043$, Mann-Whitney two-tailed analysis). Taken together, these data suggest that although elevated levels of TIMP-1 in dysplasias and carcinomas stabilize collagenous ECM in HPV16/βA-hT1$^+$ mice, they do not impede conversion of premalignant dysplasias into carcinomas, invasion of carcinomas into ectopic stroma, or metastatic spread of primary carcinomas.

TIMP-1 Potentiates Keratinocyte Hyperproliferation. Acquisition of a hyperproliferative state is an intrinsic property of many neoplastic cell types (46). Accordingly, we have reported previously that keratinocyte hyperproliferation increases incrementally during neoplastic progression in HPV16 mice and, in part, characterizes progression between premalignant stages (25, 28). In addition, we have shown that keratinocyte hyperproliferation is attenuated by ablating MMP-9 activity in HPV16 mice and as a consequence decreases the incidence of SCCs (26). Because TIMP-1 regulates MMP-9 activity *in vivo* and *in vitro* (1, 4) and inhibits tissue gelatinase activity *in vivo* (Fig. 3C), while also demonstrating mitogenicity toward keratinocytes, albeit indirectly (7, 47), we sought to determine whether the increased tumor incidence in HPV16/βA-hT1$^+$ mice was associated with an enhanced keratinocyte proliferation index or alternatively whether increased expression of TIMP-1 in HPV16 mice phenocopied our previous results with HPV16/MMP-9 homozygous null mice and attenuated keratinocyte proliferation (26). To test these hypotheses, we examined keratinocyte proliferative indices in hyperplastic, dysplastic, and SCCs and their lymphatic metastases in HPV16/βA-hT1$^+$ and control mice (Fig. 5). Qualitatively, BrdU-immunoreactivity of tissue sections suggested that in hyperplastic and dysplastic tissues of HPV16/βA-hT1$^+$ mice, a higher percentage of keratinocytes were proliferating as compared with histopathologically matched HPV16/βA-hT1$^-$ littermates at all of the neoplastic stages (data not shown). Quantification of BrdU-positive keratinocytes *in situ* supported this observation and revealed that HPV16/βA-hT1$^+$ keratinocytes in early hyperplastic tissue (1 month of age) attained a hyperproliferative state (23.9% in HPV16/βA-hT1$^+$ *versus* 16.3% in HPV16/βA-hT1$^-$; $P = 0.023$, Mann-Whitney) more commonly associated with later dysplastic tissue characteristic of 6-month-old transgenic HPV16/βA-hT1$^-$ animals (Fig. 5*A*). At the later time point in dysplastic HPV16/βA-hT1$^+$ skin, hyperproliferation indices more resembled carcinomas than dysplastic epidermis (24.1% in HPV16/βA-hT1$^+$ *versus* 18.5% in HPV16/βA-hT1$^-$; $P = 0.014$, Mann-Whitney); however, after malignant conversion, differences between the two genotypes were indistinguishable (Fig. 5*A*).

To determine how transgenic expression of hTIMP-1 regulates the observed keratinocyte hyperproliferation *in vivo* in premalignant

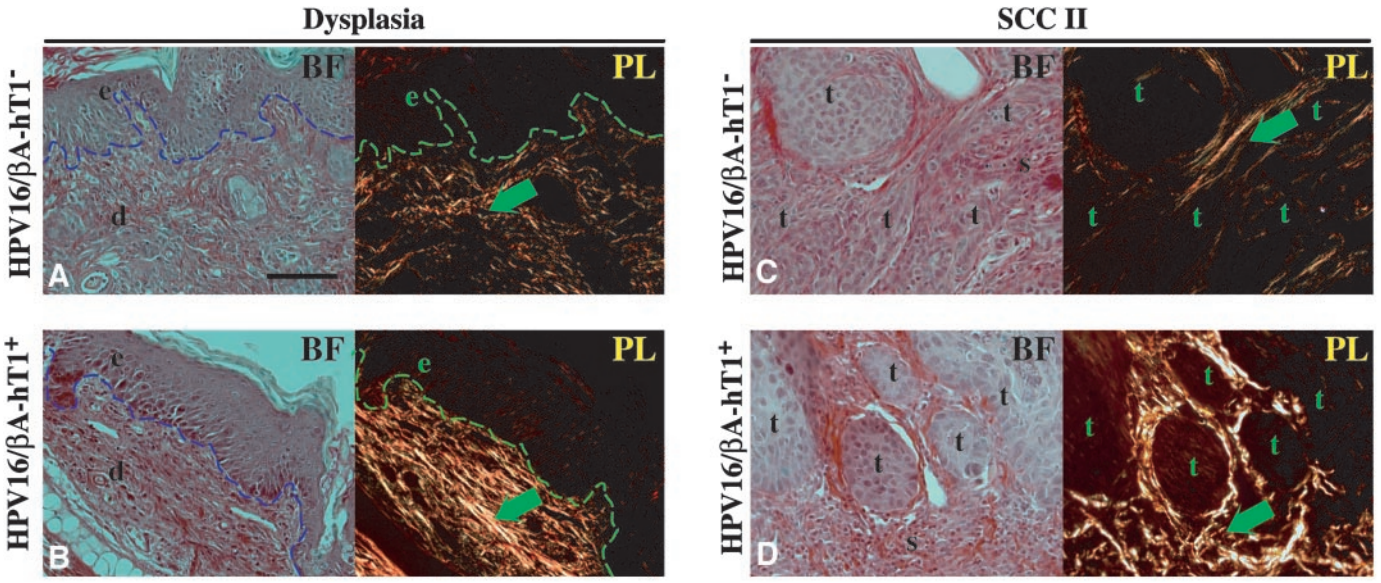

Fig. 4. Increased levels of tissue inhibitor of metalloproteinase (TIMP)-1 stabilize collagenous matrices. *A–D*, stabilization of collagen matrix in human papillomavirus-16 (HPV16)/βA-hT1$^+$ mice. Picrosirius red staining was performed on tissue sections from premalignant ears with dysplasia (*A* and *B*), and squamous cell carcinoma (*SCC*) Grade II pathologies (*C* and *D*) from HPV16/βA-hT1$^-$ (*A* and *C*) and HPV16/βA-hT1$^+$ (*B* and *D*) mice. Brightfield (*BF*) images indicate histologic structure, whereas polarized light (*PL*) images reveal mature collagen as bright orange fibers, denoted by *green arrows*. *Dashed lines* indicate the epidermal-dermal boundaries; e, epidermis; d, dermis; t, tumor; and s, stroma. Scale bar: 100 μm (*A–D*).

HPV16/βA-hT1$^+$ skin, we sought to determine whether hTIMP-1 regulated proliferation of mouse keratinocytes in culture directly. In agreement with previous reports (7, 47), our analyses revealed that hTIMP-1 protein alone was insufficient to induce a mitogenic response in immortalized murine keratinocytes, but it potentiated keratinocyte proliferation and entry into S-phase when provided in the presence of mouse epidermal growth factor (data not shown). These data suggest that TIMP-1 induces keratinocyte hyperproliferation *in vitro* (and *in vivo*) by indirect mechanisms.

Cell number in tissues increases only when the proliferative index is not balanced by an increased apoptotic index. Because TIMP-1 may regulate apoptosis in some contexts, we asked whether the increased proliferative index observed in HPV16/βA-hT1$^+$ mice was caused by an altered apoptotic frequency (48, 49). Accordingly, keratinocyte apoptotic index was quantified using the terminal deoxynucleotidyl transferase-mediated nick end labeling assay on staged neoplastic tissue sections adjacent to those used previously to assess proliferation and revealed that apoptotic indices were similar in HPV16/βA-hT1$^+$ mice and their littermate controls in all of the stages of neoplastic development in histopathologically matched sections (Fig. 5*B*). Taken together, these data imply that the increased proliferation index observed during early neoplastic progression in HPV16/βA-hT1$^+$ was the result of the mitogenic properties, direct or indirect, of TIMP-1 and independent of apoptotic cell death by TIMP-1 in this system.

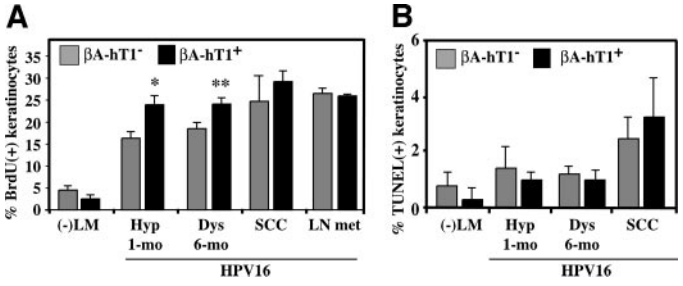

Fig. 5. Low-level tissue inhibitor of metalloproteinase (*TIMP*)-1 expression potentiates keratinocyte hyperproliferation in human papillomavirus-16 (*HPV16*)/βA-hT1$^+$ mice. *A*, proliferation of keratinocytes during neoplastic progression. Keratinocyte proliferation was assessed in paraffin-embedded ear and squamous cell carcinoma (*SCC*) tissue sections from negative littermate (*−LM*), HPV16/βA-hT1$^-$, and HPV16/βA-hT1$^+$ mice at distinct stages of neoplastic progression (*e.g.*, 1-month-old mice with hyperplastic ears, 6-month-old mice with dysplastic ears, and in SCCs). Dual-color immunohistochemistry for immunoreactivity of bromodeoxyuridine (*BrdU*) and keratin intermediate filaments was performed on tissue sections. Keratinocyte proliferative index was determined as the percentage of BrdU-positive keratinocytes as a fraction of total keratinocytes (% BrdU + keratinocytes) averaged from five high-power fields per mouse and five mice per category. Error bars represent SE, and *asterisks* indicate statistically significant differences between HPV16/βA-hT1$^-$ and HPV16/βA-hT1$^+$ categories ($*P = 0.0228$; $**P = 0.0140$, Mann-Whitney). *B*, keratinocyte apoptotic index. The terminal deoxynucleotidyl transferase-mediated nick end labeling (*TUNEL*) reaction was performed on adjacent tissue sections to those used in (*A*) to determine the percentage of TUNEL-positive keratinocytes at distinct stages of neoplastic development in the two cohorts of mice. Apoptotic index was quantified as the percentage of TUNEL-positive keratinocytes over total keratinocytes averaged from five high-power fields per mouse and five mice per category, and no statistically significant differences were found between the respective categories.

Because TIMP-1 can regulate recruitment of inflammatory cells and activation of angiogenesis in some contexts (4, 32), and because we have previously reported inflammation and angiogenesis to be rate-limiting stage-specific characteristics of neoplastic progression in HPV16 transgenic mice (26, 27, 50), we also assessed the profile of inflammatory cells infiltrating neoplastic tissue (*e.g.*, mast cells and neutrophils) and onset and organization of angiogenic vasculature during neoplastic progression. We found no quantifiable difference by any of the parameters tested at 1 month, 4 months, and 6 months and in carcinomas of HPV16/βA-hT1$^+$ and HPV16/βA-hT1$^-$ mice (data not shown). Our interpretation of these data is that increased tumorgenicity in HPV16/βA-hT1$^+$ mice results from keratinocyte hyperproliferation caused by chronic expression of hTIMP-1 in (at-risk) early neoplastic keratinocytes.

Accelerated Onset of Genomic Instability in Hyperplastic HPV16/βA-hT1$^+$ Mice. Recurrent genome copy number aberrations in proliferating neoplastic cells are a common feature of human and murine cancers and are believed to contribute to tumor evolution by copy number-induced alterations in gene expression (51–53). Using array-based comparative genomic hybridization analysis to examine the complexity of genomic copy number changes associated with epithelial carcinogenesis in HPV16 mice, we found recurrent copy number gains on chromosome 5 in 80% of SCCs, whereas copy

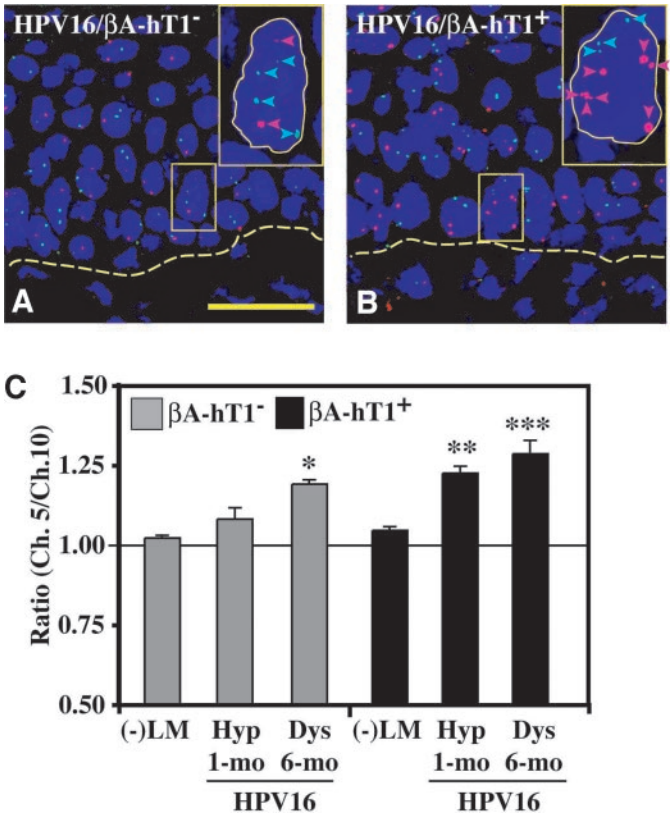

Fig. 6. Tissue inhibitor of metalloproteinase (TIMP)-1 expression induces early onset of chromosomal aberrations in hyperplastic human papillomavirus-16 (HPV16)/βA-hT1$^+$ keratinocytes. *A* and *B*, dual-color fluorescence *in situ* hybridization (FISH) using DNA probes specific for either chromosome 5 (*red staining*) or chromosome 10 (*green staining*) was performed on 1-month-old hyperplastic ear tissue sections from HPV16/βA-hT1$^-$ (*A*) and HPV16/βA-hT1$^+$ (*B*) mice. Insets show magnified nuclei from respective panels containing two FISH spots for chromosome 5 (*red arrowheads*) and four FISH spots for chromosome 10 (*green arrowheads*) in (*A*) and seven FISH spots for chromosome 5 (*red arrowheads*) and three FISH spots for chromosome 10 (*green arrowheads*) in (*B*). Scale bar: 50 μm (*A* and *B*). *C*, quantification of FISH was performed on tissue sections of neoplastic ears (ages 1 month and 6 months) and compared with skin from normal negative littermates (−LM), respectively. Values represent the ratio of the copy number for chromosome 5 over the copy number for chromosome 10 assessed from 50 nuclei per mouse and averaged from four to six mice per category. Error bars represent SE, and *asterisks* denote statistically significant differences (*−LM βA-hT1$^-$ *versus* 6-month-old HPV16/βA-hT1$^-$; $P = 0.0095$, Mann-Whitney; **−LM βA-hT1$^+$ *versus* 1-month-old HPV16/βA-hT1$^+$; $P = 0.0286$, Mann-Whitney; and ***−LM βA-hT1$^+$ *versus* 6-month-old HPV16/βA-hT1$^+$; $P = 0.0159$, Mann-Whitney).

number changes on chromosome 10 are rare and occur in fewer than 1% of carcinomas examined ($n = 30$).[6] Because low-level expression of TIMP-1 in early premalignant tissue potentiates keratinocyte hyperproliferation, we determined whether it also might potentiate appearance of an aneuploid genotype and thereby enhance malignant risk. We used dual-color FISH analysis with markers for chromosome 5 and chromosome 10 on hyperplastic and dysplastic tissue sections from 1-month-old and 6-month-old HPV16/βA-hT1$^+$ and HPV16/βA-hT1$^-$ mice (Fig. 6). Fifty FISH measurements were taken from each tissue; four to six tissues were examined for each histopathologic stage; and two independent loci were examined for each chromosome.

Chromosome 5 and 10 FISH analysis of nuclei in 1-month-old hyperplastic HPV16/βA-hT1$^-$ keratinocytes showed a negligible increase in chromosome 5 signals relative to chromosome 10 compared with nuclei in negative littermate diploid control tissue, whereas nuclei of 6-month-old dysplastic keratinocytes in HPV16/βA-hT1$^-$ tissue showed a significant relative increase in chromosome 5 signals ($P = 0.0095$, Mann-Whitney two-tailed) compared with the same negative littermate control tissue (Fig. 6, *A* and *C*). In contrast, chromosome 5 and 10 FISH analysis of 1-month-old HPV16/βA-hT1$^+$ hyperplasias revealed a significant relative increase of chromosome 5 signals ($P = 0.0286$, Mann-Whitney two-tailed) that became more pronounced in later dysplastic keratinocytes ($P = 0.0159$, Mann-Whitney two-tailed; Fig. 6*C*). The increased copy number level of chromosome 5 in hyperplastic HPV16/βA-hT1$^+$ epidermis ranged from three to seven copies (Fig. 6*B*, inset), suggesting that chromosomal aberrations, observed more typically in dysplastic keratinocytes of older HPV16 transgenic mice (age 6 months), occur at an earlier age and stage in HPV16/βA-hT1$^+$ mice coincident with increased keratinocyte hyperproliferation in 1-month hyperplastic epidermis.

DISCUSSION

The present study reveals that TIMP-1 functionally contributes to epithelial cancer development in tumor-prone transgenic mice and is not regulated coordinately with other TIMP family members. We found that TIMP-1 enhanced keratinocyte hyperproliferation and accelerated appearance of genomic copy number abnormalities in early premalignant cells, thereby enhancing their susceptibility to undergo malignant conversion. In addition, in fully malignant tissue, TIMP-1 effectively inhibited (MMP) gelatinolytic activity and stabilized collagen matrices *in vivo* but did not inhibit invasion of malignant cells into ectopic tissue compartments or metastatic spread of primary carcinomas. The combined implications of these data are that TIMP-1 can enhance neoplastic risk while also stabilizing tumor stroma, and provide additional evidence that late-stage therapies mimicking TIMP-1 inhibition of MP activity will have limited clinical efficacy.

TIMP-1 and Inhibition of MP Activity. Enzymes that initiate remodeling of the ECM have long been viewed as essential for tumor development (54–56). Neoplastic cells were thought initially to produce these enzymes, thus permitting invasion into ectopic tissues, entry and exit from vasculature, and metastasis to distant organs. MMPs were prime candidates for these activities because MMP family members degrade collectively all of the structural components of the ECM (*in vitro*) and were found to have increased expression and activity in tissues undergoing various types of pathologic remodeling, including cancer (57). Additional evidence supporting the hypothesis that MMPs were critical regulators of invasion and metastasis came from studies of their natural tissue inhibitors, TIMPs. Several groups demonstrated that either overexpression of TIMPs or i.p. injection of recombinant TIMP-1 reduced experimental metastasis formation (58–63), whereas functional studies exploiting transgenic technology additionally revealed TIMP/MMP significance during carcinogenesis (*e.g.*, TIMP-1 overproduction slowed chemical carcinogenesis in skin; Ref. 64) and inhibited SV40 large T antigen-induced liver (65) and MMP-3/stromelysin-induced mammary carcinogenesis (20, 66). However, paradoxically elevated TIMP-1 mRNA expression also was reported to correlate with malignant progression and poor clinical prognosis of several human cancers (12, 67, 68).

To determine whether increased TIMP-1 expression would slow *de novo* carcinogenesis as hypothesized initially or alternatively potentiate carcinogenesis as suggested by observations associating TIMP-1 with poor clinical outcome, we took a genetic approach using a mouse model of epithelial carcinogenesis harboring a TIMP-1 transgene. Results from the current study provide insight into the duality of TIMP-1 as a modifier of neoplastic progression and highlight the irrelevance of inhibiting MMP activity once tumors have already formed. Expression of TIMP-1 in malignant lesions of HPV16 mice is an efficacious inhibitor of gelatinase activity (Fig. 3) and effectively stabilizes collagen matrices in neoplastic tissue—effects that are consistent with TIMP-1 acting as an MP inhibitor. However, the net

[6] R. Diaz and L. M. Coussens, unpublished observations.

effect of these bioactivities is without consequence in limiting malignant conversion, malignant growth, or metastatic spread of carcinomas—results that are remarkably similar to those reported for human clinical trials testing the efficacy of MP inhibitors in patients with late-stage neoplastic disease (69, 70), for whom treatment with synthetic MP inhibitors generally failed to show any benefit compared with placebo in terms of overall survival or time to progression (71, 72).

Heppner-Goss *et al.* (24) compared the effects of transgenic TIMP-1 expression in a mouse model of intestinal neoplasia and found that TIMP-1 enhanced tumor multiplicity; however, when those same mice were treated throughout neoplastic progression with batimastat, a broad spectrum MP inhibitor (73), there was a reduction in tumorgenicity (24). This seeming paradox can be explained because TIMP-1 is a multifunctional protein whose activities include inhibition of MP activity at high concentration as opposed to mitogenic activities at lower concentrations (2, 74), in contrast to batimastat, which functions primarily as an MP inhibitor. One interpretation of these data is that inhibiting MP activity may be more efficacious if performed before the emergence of malignant disease. This hypothesis has been borne out by Bergers *et al.* (75), who reported that treatment of pancreatic islet carcinomas with batimastat was without effect on the persistence or continued growth of malignant tumors, whereas treatment of precursor hyperplastic lesions reduced their progression into more advanced angiogenic dysplasias, suggesting that the effective window for targeting MP activity as an anticancer strategy is early in the neoplastic cascade. When combined with functional studies examining transgenic mouse models of *de novo* carcinogenesis harboring homozygous null mutations in individual MMP genes (26, 76, 77), the implication is that targeting MPs with synthetic inhibitors devoid of mitogenic bioactivity would yield more desirable outcomes if performed before overt tumor formation.

Procancer Activities of TIMP-1: Proliferation and Chromosome Instability. If TIMP-1 effectively inhibits MP activity *in vivo*, why then is enhanced expression of hTIMP-1 protumorigenic? Our findings suggest that induction of hyperproliferation *versus* regulation of ECM remodeling are stage- and concentration-dependent responses to TIMP-1 in HPV16 transgenic mice and represent *in vivo* evidence supporting procancer roles for TIMP-1 during carcinogenesis.

Previous reports using *in vitro* cell-based assays have demonstrated (indirect) mitogenic properties of TIMP-1 in a wide range of cell types (6, 8), including keratinocytes (7, 47), and using altered non-MMP inhibitory versions of TIMP-1, others have shown that TIMP-1's mitogenic properties are separate and distinct from its MMP inhibitory capabilities (9, 12). Moreover, in addition to interacting with MPs, TIMP-1 binds to a non-MP cell surface protein with high affinity (K_d = 100 pM; Ref. 8). Diverse mechanisms have been suggested for how TIMP-1 may induce proliferation *in vivo* in addition to its indirect mitogenic properties (7, 8, 12, 47, 78). In a mammary carcinoma transplantation model, TIMP-1 expression correlated with enhanced epithelial proliferation largely because of increased expression of VEGF-A mRNA and subsequent enhanced angiogenesis (79). In contrast, using lymphoma cells, TIMP-1 was found to stimulate tumor growth by reciprocally decreasing apoptotic indices (80). Paradoxically, in a mouse model of intestinal neoplasia (*e.g., min* mice), enhanced TIMP-1 expression resulted in increased tumor multiplicity; however, changes in the proliferative status of neoplastic cells and angiogenesis were not examined (24).

Proteolytic activity of MMPs and other MP families (*e.g.,* ADAMs and/or ADAM-TS members) has been linked to regulation of proliferation via proteolytic activation of growth inhibitory molecules, such as transforming growth factor-β, and activation of growth-promoting factors (*e.g.,* insulin-like growth factor ligands and members of the epidermal growth factor family; Refs. 4 and 57). As such, it is reasonable to conclude that in addition to TIMP-1 exerting indirect mitogenic activity *in vivo* and in cell-based assays *in vitro*, the possibility cannot be ruled out that at low concentrations (*e.g.,* during early neoplastic progression), TIMP-1 regulates the bioactivity of a growth-restricting factor whose inhibition releases keratinocyte proliferative potential.

Regardless of the mechanism, how does increased hyperproliferative activity caused by TIMP-1 translate into increased tumorgenicity in HPV16 mice or in mice predisposed to intestinal neoplasia? Mechanisms linking cell division and aneuploidy have been well characterized (81, 82) and include, for example, errors in chromosome segregation during mitosis caused by aberrant centrosome duplication (83, 84). Regarding mechanisms of carcinogenesis resulting from HPV-induced tumorgenicity, it has been reported that the HPV oncoprotein E7 induces cell division-associated aneuploidy by enhancing the activity of cdk2/cyclin E and cdk2/cyclin A complexes, both of which are involved in regulating centrosome duplication *in vivo* (85). Thus, when the potential for chromosomal instability has been primed (by E7-induced centrosome errors), our data support a model in which low-level expression of TIMP-1 enhances keratinocyte hyperproliferation and results in a higher fraction of aneuploid cells at risk to undergo malignant conversion caused by earlier accumulation of E7-induced chromosomal aberrations. Perhaps in human cancers, as in the HPV16 and *min* mouse models, late-stage MP inhibition and ECM stabilization are not sufficient to block neoplastic cells that already have been programmed genomically, resulting in loss of cell cycle checkpoint control, hyperproliferation, and other events involved in malignant conversion. Premalignant chromosomal aberrations have been detected in several human malignancies (86–88), and notably early head and neck SCCs provide a predictive value for malignant conversion (89, 90). Taken together and in conjunction with results from the present study, we suggest that of the many events that must take place to produce a *bone fide* tumor, intrinsic genomic changes involved in manifesting cancer likely occur at an early stage in the evolutionary process and, in part, set the stage for additional deregulation of cell intrinsic events involved in carcinogenesis. In HPV16 mice at least, genomic aberrations could represent one of these intrinsic neoplastic events subject to regulation by TIMP-1-induced hyperproliferation. Given the observation that TIMP-1 assumes a nuclear localization after plasma membrane binding in some cell types (91, 92), we cannot rule out the possibility that TIMP-1 also may affect directly (or indirectly) chromosome integrity in E6/E7-positive keratinocytes in HPV16 mice; however, examining this possibility awaits generation of reagents capable of detecting TIMP-1 protein localization *in situ*.

Multiplicity of Pathways in HPV16 Mice. If increased TIMP-1 potentiates neoplastic risk, does homozygous loss of TIMP-1 attenuate that same risk? We addressed this question by intercrossing HPV16 mice into a TIMP-1 homozygous null background (93) and found no discernible difference between HPV16/T1$^{-/-}$ (n = 109) and HPV16/T1$^{+/-}$ (n = 51) cohorts.[6] Our interpretation of this seeming disparity illuminates the functional contribution of TIMP-1 as a modifier of carcinogenesis that is sufficient but is not necessary for promoting the multiplicity of changes occurring during tumor development. We hypothesize that these data support a model reflecting the fact that multiple discrete pathways must be altered and/or activated for full progression to the tumor state and, furthermore, that a minimal number or combination of these pathways must be compromised to exert a detectable attenuation in tumorigenesis. Hence, one implication of this is that factors such as MMP-9 would participate in multiple pathways, whereas conversely TIMP-1 exerts regulatory pressure on fewer pathways necessary for manifesting a tumor. In

conclusion, the findings described here suggest that during *de novo* epithelial carcinogenesis, TIMP-1 functionally enhances neoplastic progression. Hence, therapeutic strategies based on exploiting TIMP-type bioactivity during late-stage disease may not only be of limited efficacy but also may result potentially in increased presence of malignant-prone cells.

ACKNOWLEDGMENTS

We thank Zena Werb for providing βA-hT1$^+$ transgenic mice; Jake Lee and Andre Whitkin for technical assistance; and Joe Gray, Zena Werb, Koei Chin, and members of the Coussens laboratory for fruitful discussion and critical comments.

REFERENCES

1. Woessner, J. F., and Nagase, H. Matrix Metalloproteinases and TIMPs. Oxford, UK: Oxford University Press, 2000.
2. Brew, K., Dinakarpandian, D., and Nagase, H. Tissue inhibitors of metalloproteinases: evolution, structure and function. Biochim. Biophys. Acta, *1477:* 267–283, 2000.
3. Fassina, G., Ferrari, N., Brigati, C., Benelli, R., Santi, L., Noonan, D. M., and Albini, A. Tissue inhibitors of metalloproteases: regulation and biological activities. Clin. Exp. Metastasis, *18:* 111–120, 2000.
4. Lafleur, M. A., Handsley, M. M., and Edwards, D. R. Metalloproteinases and their inhibitors in angiogenesis. Exp. Rev. Mol. Med., *5:* 1–39, 2003.
5. Docherty, A. J., Lyons, A., Smith, B. J., Wright, E. M., Stephens, P. E., Harris, T. J., Murphy, G., and Reynolds, J. J. Sequence of human tissue inhibitor of metalloproteinases and its identity to erythroid-potentiating activity. Nature (Lond.), *318:* 66–69, 1985.
6. Hayakawa, T., Yamashita, K., Tanzawa, K., Uchijima, E., and Iwata, K. Growth-promoting activity of tissue inhibitor of metalloproteinases-1 (TIMP-1) for a wide range of cells. A possible new growth factor in serum. FEBS Lett., *298:* 29–32, 1992.
7. Bertaux, B., Hornebeck, W., Eisen, A. Z., and Dubertret, L. Growth stimulation of human keratinocytes by tissue inhibitor of metalloproteinases. J. Investig. Dermatol., *97:* 679–685, 1991.
8. Avalos, B. R., Kaufman, S. E., Tomonaga, M., Williams, R. E., Golde, D. W., and Gasson, J. C. K562 cells produce and respond to human erythroid-potentiating activity. Blood, *71:* 1720–1725, 1988.
9. Chesler, L., Golde, D. W., Bersch, N., and Johnson, M. D. Metalloproteinase inhibition and erythroid potentiation are independent activities of tissue inhibitor of metalloproteinases-1. Blood, *86:* 4506–4515, 1995.
10. Yamada, E., Tobe, T., Yamada, H., Okamoto, N., Zack, D. J., Werb, Z., Soloway, P. D., and Campochiaro, P. A. TIMP-1 promotes VEGF-induced neovascularization in the retina. Histol. Histopathol., *16:* 87–97, 2001.
11. Thorgeirsson, U. P., Yoshiji, H., Sinha, C. C., and Gomez, D. E. Breast cancer; tumor neovasculature and the effect of tissue inhibitor of metalloproteinases-1 (TIMP-1) on angiogenesis. In Vivo, *10:* 137–144, 1996.
12. Guedez, L., Mansoor, A., Birkedal-Hansen, B., Lim, M. S., Fukushima, P., Venzon, D., Stetler-Stevenson, W. G., and Stetler-Stevenson, M. Tissue inhibitor of metalloproteinases 1 regulation of interleukin-10 in B-cell differentiation and lymphomagenesis. Blood, *97:* 1796–1802, 2001.
13. Apparailly, F., Noel, D., Millet, V., Baker, A. H., Lisignoli, G., Jacquet, C., Kaiser, M. J., Sany, J., and Jorgensen, C. Paradoxical effects of tissue inhibitor of metalloproteinases 1 gene transfer in collagen-induced arthritis. Arthritis Rheum., *44:* 1444–1454, 2001.
14. Kruger, A., Sanchez-Sweatman, O. H., Martin, D. C., Fata, J. E., Ho, A. T., Orr, F. W., Ruther, U., and Khokha, R. Host TIMP-1 overexpression confers resistance to experimental brain metastasis of a fibrosarcoma cell line. Oncogene, *16:* 2419–2423, 1998.
15. Valente, P., Fassina, G., Melchiori, A., Masiello, L., Cilli, M., Vacca, A., Onisto, M., Santi, L., Stetler-Stevenson, W. G., and Albini, A. TIMP-2 over-expression reduces invasion and angiogenesis and protects B16F10 melanoma cells from apoptosis. Int. J. Cancer, *75:* 246–253, 1998.
16. Smith, M. R., Kung, H., Durum, S. K., Colburn, N. H., and Sun, Y. TIMP-3 induces cell death by stabilizing TNF-á receptors on the surface of human colon carcinoma cells. Cytokine, *9:* 770–780, 1997.
17. Jiang, Y., Wang, M., Celiker, M. Y., Liu, Y. E., Sang, Q. X., Goldberg, I. D., and Shi, Y. E. Stimulation of mammary tumorigenesis by systemic tissue inhibitor of matrix metalloproteinase 4 gene delivery. Cancer Res., *61:* 2365–2370, 2001.
18. Curran, S., and Murray, G. I. Matrix metalloproteinases in tumour invasion and metastasis. J. Pathol., *189:* 300–308, 1999.
19. Martin, D. C., Sanchez-Sweatman, O. H., Ho, A. T., Inderdeo, D. S., Tsao, M. S., and Khokha, R. Transgenic TIMP-1 inhibits simian virus 40 T antigen-induced hepatocarcinogenesis by impairment of hepatocellular proliferation and tumor angiogenesis. Lab. Invest., *79:* 225–234, 1999.
20. Sternlicht, M. D., Lochter, A., Sympson, C. J., Huey, B., Rougier, J. P., Gray, J. W., Pinkel, D., Bissell, M. J., and Werb, Z. The stromal proteinase MMP3/stromelysin-1 promotes mammary carcinogenesis. Cell, *98:* 137–146, 1999.
21. Noritake, H., Miyamori, H., Goto, C., Seiki, M., and Sato, H. Overexpression of tissue inhibitor of matrix metalloproteinases-1 (TIMP-1) in metastatic MDCK cells transformed by v-*src*. Clin. Exp. Metastasis, *17:* 105–110, 1999.
22. Kawamata, H., Kawai, K., Kameyama, S., Johnson, M. D., Stetler-Stevenson, W. G., and Oyasu, R. Over-expression of tissue inhibitor of matrix metalloproteinases (TIMP1 and TIMP2) suppresses extravasation of pulmonary metastasis of a rat bladder carcinoma. Int. J. Cancer, *63:* 680–687, 1995.
23. Watanabe, M., Takahashi, Y., Ohta, T., Mai, M., Sasaki, T., and Seiki, M. Inhibition of metastasis in human gastric cancer cells transfected with tissue inhibitor of metalloproteinase 1 gene in nude mice. Cancer (Phila.), *77:* 1676–1680, 1996.
24. Heppner-Goss, K. J., Brown, P. D., and Matrisian, L. M. Differing effects of endogenous and synthetic inhibitors of metalloproteinases on intestinal tumorigenesis. Int. J. Cancer, *78:* 629–635, 1998.
25. Coussens, L. M., Hanahan, D., and Arbeit, J. M. Genetic predisposition and parameters of malignant progression in K14-HPV16 transgenic mice. Am. J. Pathol., *149:* 1899–1917, 1996.
26. Coussens, L. M., Tinkle, C. L., Hanahan, D., and Werb, Z. MMP-9 supplied by bone marrow-derived cells contributes to skin carcinogenesis. Cell, *103:* 481–490, 2000.
27. van Kempen, L. C. L., Rhee, J. S., Dehne, K., Lee, J., Edwards, D. R., and Coussens, L. M. Epithelial carcinogenesis: dynamic interplay between neoplastic cells and their microenvironment. Differentiation, *70:* 501–623, 2002.
28. Arbeit, J. M., Munger, K., Howley, P. M., and Hanahan, D. Progressive squamous epithelial neoplasia in K14-human papillomavirus type 16 transgenic mice. J. Virol., *68:* 4358–4368, 1994.
29. Daniel, D., Meyer-Morse, N., Bergsland, E. K., Dehne, K., Coussens, L. M., and Hanahan, D. Immune enhancement of skin carcinogenesis by CD4$^+$ T cells. J. Exp. Med., *197:* 1017–1028, 2003.
30. Alexander, C. M., Howard, E. W., Bissell, M. J., and Werb, Z. Rescue of mammary epithelial cell apoptosis and entactin degradation by a tissue inhibitor of metalloproteinases-1 transgene. J. Cell Biol., *135:* 1669–1677, 1996.
31. Chomczynski, P. A reagent for the single-step simultaneous isolation of RNA, DNA and proteins from cell and tissue samples. Biotechniques, *15:* 532–534, 536–537, 1993.
32. Edwards, D. R. The tissue inhibitors of metalloproteinases (TIMPs). *In:* N. J. Clendeninn and K. Appelt (eds.), Matrix Metalloproteinase Inhibitors in Cancer Therapy, pp. 67–84. Totowa, NJ: Humana Press, 2000.
33. Shimizu, S., Malik, K., Sejima, H., Kishi, J., Hayakawa, T., and Koiwai, O. Cloning and sequencing of the cDNA encoding a mouse tissue inhibitor of metalloproteinase-2. Gene, *114:* 291–292, 1992.
34. Apte, S. S., Hayashi, K., Seldin, M. F., Mattei, M. G., Hayashi, M., and Olsen, B. R. Gene encoding a novel murine tissue inhibitor of metalloproteinases (TIMP), TIMP-3, is expressed in developing mouse epithelia, cartilage, and muscle, and is located on mouse chromosome 10. Dev. Dyn., *200:* 177–197, 1994.
35. Leco, K. J., Apte, S. S., Taniguchi, G. T., Hawkes, S. P., Khokha, R., Schultz, G. A., and Edwards, D. R. Murine tissue inhibitor of metalloproteinases-4 (Timp-4): cDNA isolation and expression in adult mouse tissues. FEBS Lett., *401:* 213–217, 1997.
36. Herron, G. S., Werb, Z., Dwyer, K., and Banda, M. J. Secretion of metalloproteinases by stimulated capillary endothelial cells. I. Production of procollagenase and prostromelysin exceeds expression of proteolytic activity. J. Biol. Chem., *261:* 2810–2813, 1986.
37. Herron, G. S., Banda, M. J., Clark, E. J., Gavrilovic, J., and Werb, Z. Secretion of metalloproteinases by stimulated capillary endothelial cells. II. Expression of collagenase and stromelysin activities is regulated by endogenous inhibitors. J. Biol. Chem., *261:* 2814–2818, 1986.
38. Canham, P. B., Finlay, H. M., Kiernan, J. A., and Ferguson, G. G. Layered structure of saccular aneurysms assessed by collagen birefringence. Neurol. Res., *21:* 618–626, 1999.
39. Junqueira, L. C., Bignolas, G., and Brentani, R. R. Picrosirius staining plus polarization microscopy, a specific method for collagen detection in tissue sections. Histochem. J., *11:* 447–455, 1979.
40. Puchtler, H., Waldrop, F. S., and Valentine, L. S. Polarization microscopic studies of connective tissue stained with piscro-sirius red FBA. Beitr. Pathol., *150:* 174–187, 1973.
41. Junqueira, L. C., Cossermelli, W., and Brentani, R. Differential staining of collagens type I, II and III by Sirius Red and polarization microscopy. Arch. Histol. Jpn., *41:* 267–274, 1978.
42. Malkusch, W., Rehn, B., and Bruch, J. Advantages of Sirius Red staining for quantitative morphometric collagen measurements in lungs. Exp. Lung Res., *21:* 67–77, 1995.
43. Polette, M., Clavel, C., Birembaut, P., and De Clerck, Y. A. Localization by *in situ* hybridization of mRNAs encoding stromelysin 3 and tissue inhibitors of metalloproteinases TIMP-1 and TIMP-2 in human head and neck carcinomas. Pathol. Res. Pract., *189:* 1052–1057, 1993.
44. Charous, S. J., Stricklin, G. P., Nanney, L. B., Netterville, J. L., and Burkey, B. B. Expression of matrix metalloproteinases and tissue inhibitor of metalloproteinases in head and neck squamous cell carcinoma. Ann. Otol. Rhinol. Laryngol., *106:* 271–278, 1997.
45. Vaalamo, M., Leivo, T., and Saarialho-Kere, U. Differential expression of tissue inhibitors of metalloproteinases (TIMP-1, -2, -3, and -4) in normal and aberrant wound healing. Hum. Pathol., *30:* 795–802, 1999.
46. Hanahan, D., and Weinberg, R. A. The hallmarks of cancer. Cell, *100:* 57–70, 2000.
47. Buisson-Legendre, N., Emonard, H., Bernard, P., and Hornebeck, W. Relationship between cell-associated matrix metalloproteinase 9 and psoriatic keratinocyte growth. J. Investig. Dermatol., *115:* 213–218, 2000.
48. Guedez, L., Stetler-Stevenson, W. G., Wolff, L., Wang, J., Fukushima, P., Mansoor, A., and Stetler-Stevenson, M. *In vitro* suppression of programmed cell death of B cells by tissue inhibitor of metalloproteinases-1. J. Clin. Investig., *102:* 2002–2010, 1998.

49. Li, G., Fridman, R., and Kim, H. R. Tissue inhibitor of metalloproteinase-1 inhibits apoptosis of human breast epithelial cells. Cancer Res., *59:* 6267–6275, 1999.
50. Coussens, L. M., Raymond, W. W., Bergers, G., Laig-Webster, M., Behrendtsen, O., Werb, Z., Caughey, G. H., and Hanahan, D. Inflammatory mast cells up-regulate angiogenesis during squamous epithelial carcinogenesis. Genes Dev., *13:* 1382–1397, 1999.
51. Pinkel, D., Segraves, R., Sudar, D., Clark, S., Poole, I., Kowbel, D., Collins, C., Kuo, W. L., Chen, C., Zhai, Y., Dairkee, S. H., Ljung, B. M., Gray, J. W., and Albertson, D. G. High resolution analysis of DNA copy number variation using comparative genomic hybridization to microarrays. Nat. Genet., *20:* 207–211, 1998.
52. Hodgson, G., Hager, J. H., Volik, S., Hariono, S., Wernick, M., Moore, D., Nowak, N., Albertson, D. G., Pinkel, D., Collins, C., Hanahan, D., and Gray, J. W. Genome scanning with array CGH delineates regional alterations in mouse islet carcinomas. Nat. Genet., *29:* 459–464, 2001.
53. Snidjers, A. M., Nowee, M., Fridlyand, J., Piek, J., Dorsman, J. C., Pinkel, D., van Diest, P. J., Verheijen, J. H., and Albertson, D. G. Genome-wide-array-based comparative genomic hybridization reveals genetic homogeneity and frequent copy number increases encompassing CCNE1 in fallopian tube carcinoma. Oncogene *22:* 4281–4286, 2003.
54. Brinckerhoff, C. E., and Matrisian, L. Matrix metalloproteinases: a tail of a frog that became a prince. Nat. Rev., *3:* 207–214, 2002.
55. Ala-aho, R., Johansson, N., Grenman, R., Fusenig, N. E., Lopez-Otin, C., and Kahari, V. M. Inhibition of collagenase-3 (MMP-13) expression in transformed human keratinocytes by interferon-ã is associated with activation of extracellular signal-regulated kinase-1, 2 and STAT1. Oncogene, *19:* 248–257, 2000.
56. Deryugina, E. I., Luo, G. X., Reisfeld, R. A., Bourdon, M. A., and Strongin, A. Tumor cell invasion through matrigel is regulated by activated matrix metalloproteinase-2. Anticancer Res., *17:* 3201–3210, 1997.
57. Egeblad, M., and Werb, Z. New functions for the matrix metalloproteinases in cancer progression. Nat. Rev. Cancer, *2:* 161–174, 2002.
58. DeClerck, Y. A., and Imren, S. Protease inhibitors: role and potential therapeutic use in human cancer. Eur. J. Cancer, *14:* 2170–2180, 1994.
59. Montgomery, A. M., Mueller, B. M., Reisfeld, R. A., Taylor, S. M., and DeClerck, Y. A. Effect of tissue inhibitor of the matrix metalloproteinases-2 expression on the growth and spontaneous metastasis of a human melanoma cell line. Cancer Res., *54:* 5467–5473, 1994.
60. Khokha, R. Suppression of the tumorigenic and metastatic abilities of murine B16–F10 melanoma cells *in vivo* by the overexpression of the tissue inhibitor of the metalloproteinases-1. J. Natl. Cancer Inst. (Bethesda), *86:* 299–304, 1994.
61. Koop, S., Khokha, R., Schmidt, E. E., MacDonald, I. C., Morris, V. L., Chambers, A. F., and Groom, A. C. Overexpression of metalloproteinase inhibitor in B16F10 cells does not affect extravasation but reduces tumor growth. Cancer Res., *54:* 4791–4797, 1994.
62. Schultz, R. M., Silberman, S., Persky, B., Bajkowski, A. S., and Carmichael, D. F. Inhibition by human recombinant tissue inhibitor of metalloproteinases of human amnion invasion and lung colonization by murine B16–F10 melanoma cells. Cancer Res., *48:* 5539–5545, 1988.
63. Alvarez, O. A., Carmichael, D. F., and DeClerck, Y. A. Inhibition of collagenolytic activity and metastasis of tumor cells by a recombinant human tissue inhibitor of metalloproteinases. J. Natl. Cancer Inst., *82:* 589–595, 1990.
64. Buck, T. B., Yoshiji, H., Harris, S. R., Bunce, O. R., and Thorgeirsson, U. P. The effects of sustained elevated levels of circulating tissue inhibitor of metalloproteinases-1 on the development of breast cancer in mice. Ann. N. Y. Acad. Sci., *878:* 732–735, 1999.
65. Martin, D. C., Rüther, U., Sanchez-Sweatman, O. H., Orr, F. W., and Khokha, R. Inhibition of SV40 T antigen-induced hepatocellular carcinoma in TIMP-1 transgenic mice. Oncogene, *13:* 569–576, 1996.
66. Sternlicht, M. D., Bissell, M. J., and Werb, Z. The matrix metalloproteinase stromelysin-1 acts as a natural mammary tumor promoter. Oncogene, *19:* 1102–1113, 2000.
67. Murashige, M., Miyahara, M., Shiraishi, N., Saito, T., Kohno, K., and Kobayashi, M. Enhanced expression of tissue inhibitors of metalloproteinases in human colorectal tumors. Jpn. J. Clin. Oncol., *26:* 303–309, 1996.
68. Schrohl, A. S., Christensen, I. J., Pedersen, A. N., Jensen, V., Mouridsen, H., Murphy, G., Foekens, J. A., Brunner, N., and Holten-Andersen, M. N. Tumor tissue concentrations of the proteinase inhibitors tissue inhibitor of metalloproteinases-1 (TIMP-1) and plasminogen activator inhibitor type 1 (PAI-1) are complementary in determining prognosis in primary breast cancer. Mol. Cell. Proteomics, *2:* 164–172, 2003.
69. Whittaker, M., Floyd, C. D., Brown, P., and Gearing, A. J. Design and therapeutic application of matrix metalloproteinase inhibitors. Chem. Rev., *99:* 2735–2776, 1999.
70. Hidalgo, M., and Eckhardt, S. G. Development of matrix metalloproteinase inhibitors in cancer therapy. J. Natl. Cancer Inst. (Bethesda), *93:* 178–193, 2001.
71. Zucker, S., Cao, J., and Chen, W. T. Critical appraisal of the use of matrix metalloproteinase inhibitors in cancer treatment. Oncogene, *19:* 6642–6650, 2000.
72. Coussens, L. M., B. Fingleton, B., and Matrisian, L. M. Matrix metalloproteinase inhibitors and cancer: trials and tribulations. Science (Wash. DC), *295:* 2387–2392, 2002.
73. Wang, X., Fu, X., Brown, P. D., Crimmin, M. J., and Hoffman, R. M. Matrix metalloproteinase inhibitor BB-94 (batimastat) inhibits human colon tumor growth and spread in a patient-like orthotopic model in nude mice. Cancer Res., *54:* 4726–4728, 1994.
74. Huang, W., Suzuki, K., Nagase, H., Arumugam, S., Van Doren, S. R., and Brew, K. Folding and characterization of the amino-terminal domain of human tissue inhibitor of metalloproteinases-1 (TIMP-1) expressed at high yield in *E. coli*. FEBS Lett., *384:* 155–161, 1996.
75. Bergers, G., Javaherian, K., Lo, K. M., Folkman, J., and Hanahan, D. Effects of angiogenesis inhibitors on multistage carcinogenesis in mice. Science (Wash. DC), *284:* 808–812, 1999.
76. Wilson, C. L., Heppner, K. J., Labosky, P. A., Hogan, B. L., and Matrisian, L. M. Intestinal tumorigenesis is suppressed in mice lacking the metalloproteinase matrilysin. Proc. Natl. Acad. Sci. USA, *94:* 1402–1407, 1997.
77. Bergers, G., Brekken, R., McMahon, G., Vu, T. H., Itoh, T., Tamaki, K., Tanzawa, K., Thorpe, P., Itohara, S., Werb, Z., and Hanahan, D. Matrix metalloproteinase-9 triggers the angiogenic switch during carcinogenesis. Nat. Cell Biol., *2:* 737–744, 2000.
78. Martin, D. C., Fowlkes, J. L., Babic, B., and Khokha, R. Insulin-like growth factor II signaling in neoplastic proliferation is blocked by transgenic expression of the metalloproteinase inhibitor TIMP-1. J. Cell Biol., *146:* 881–892, 1999.
79. Yoshiji, H., Harris, S. R., Raso, E., Gomez, D. E., Lindsay, C. K., Shibuya, M., Sinha, C. C., and Thorgeirsson, U. P. Mammary carcinoma cells over-expressing tissue inhibitor of metalloproteinases-1 show enhanced vascular endothelial growth factor expression. Int. J. Cancer, *75:* 81–87, 1998.
80. Guedez, L., McMarlin, A. J., Kingma, D. W., Bennett, T. A., Stetler-Stevenson, M., and Stetler-Stevenson, W. G. Tissue inhibitor of metalloproteinase-1 alters the tumorigenicity of Burkitt's lymphoma via divergent effects on tumor growth and angiogenesis. Am. J. Pathol., *158:* 1207–1215, 2001.
81. Doxsey, S. Duplicating dangerously: linking centrosome duplication and aneuploidy. Mol. Cell., *10:* 439–440, 2002.
82. Jallepalli, P. V., and Lengauer, C. Chromosome segregation and cancer: cutting through the mystery. Nat. Rev. Cancer, *1:* 109–117, 2001.
83. D'Assoro, A. B., Lingle, W. L., and Salisbury, J. L. Centrosome amplification and the development of cancer. Oncogene, *21:* 6146–6153, 2002.
84. Kramer, A., Neben, K., and Ho, A. D. Centrosome replication, genomic instability and cancer. Leukemia, *16:* 767–775, 2002.
85. Duensing, S., and Munger, K. Human papillomaviruses and centrosome duplication errors: modeling the origins of genomic instability. Oncogene, *21:* 6241–6248, 2002.
86. Doak, S. H., Jenkins, G. J., Parry, E. M., D'Souza, F. R., Griffiths, A. P., Toffazal, N., Shah, V., Baxter, J. N., and Parry, J. M. Chromosome 4 hyperploidy represents an early genetic aberration in premalignant Barrett's oesophagus. Gut, *52:* 623–628, 2003.
87. Duensing, S., and Munger, K. Centrosomes, genomic instability, and cervical carcinogenesis. Crit. Rev. Eukaryot. Gene. Expr., *13:* 9–23, 2003.
88. Sugai, T., Takahashi, H., Habano, W., Nakamura, S., Sato, K., Orii, S., and Suzuki, K. Analysis of genetic alterations, classified according to their DNA ploidy pattern, in the progression of colorectal adenomas and early colorectal carcinomas. J. Pathol., *200:* 168–176, 2003.
89. Bockmuhl, U., and Petersen, I. DNA ploidy and chromosomal alterations in head and neck squamous cell carcinoma. Virchows Arch., *441:* 541–550, 2002.
90. Sudbo, J., and Reith, A. Which putatively pre-malignant oral lesions become oral cancers? Clinical relevance of early targeting of high-risk individuals. J. Oral. Pathol. Med., *32:* 63–70, 2003.
91. Zhao, W. Q., Li, H., Yamashita, K., Guo, X. K., Hoshino, T., Yoshida, S., Shinya, T., and Hayakawa, T. Cell cycle-associated accumulation of tissue inhibitor of metalloproteinases-1 (TIMP-1) in the nuclei of human gingival fibroblasts. J. Cell Sci., *111* (Pt 9)*:* 1147–1153, 1998.
92. Ritter, L. M., Garfield, S. H., and Thorgeirsson, U. P. Tissue inhibitor of metalloproteinases-1 (TIMP-1) binds to the cell surface and translocates to the nucleus of human MCF-7 breast carcinoma cells. Biochem. Biophys. Res. Commun., *257:* 494–499, 1999.
93. Soloway, P. D., Alexander, C. M., Werb, Z., and Jaenisch, R. Targeted mutagenesis of Timp-1 reveals that lung tumor invasion is influenced by Timp-1 genotype of the tumor but not by that of the host. Oncogene, *13:* 2307–2314, 1996.